Solid State Communications 149 (2009) 818–821

Contents lists available at ScienceDirect

Solid State Communications

journal homepage: www.elsevier.com/locate/ssc

Graphitization of activated carbon under high pressures and high temperatures

J.G. Zhao *, F.Y. Li, C.Q. Jin

Beijing National Lab for Condensed Matter Physics, Institute of Physics, Chinese Academy of Sciences, Beijing 100080, PR China

ARTICLE INFO

Article history:
Received 29 April 2007
Received in revised form
6 November 2007
Accepted 15 December 2008
by C.H.R. Thomsen
Available online 25 December 2008

PACS:
62.50.+p
61.66.Bi
61.10.-i

Keywords:
A. Activated carbon
B. High-pressure sintering
D. Graphitization

ABSTRACT

Activated carbon was treated at 5.0 GPa up to 1600 °C and the structural evolution in the graphitization process was investigated. The graphitization temperature is reduced to 1200 °C at 5 GPa, as reflected by x-ray diffraction patterns. Honeycomb-like structures come into being in the high-pressure sintering temperature range of 1000–1100 °C and slice-like structures appear after graphitization. Raman frequency and half width drop drastically near the graphitization temperature, and the appearance of D and D′ lines indicates there are still some disorder structures in the graphitized activated carbon.

1. Introduction

Carbon has attracted more and more attention in scientific aspects and technological applications due to the diversity of structural and electrical properties. The forms of carbon include not only the crystalline phase of graphite, diamond and fullerene, but also some amorphous materials [1]. Recently, some interesting phenomena on carbon-based materials have been found: ferromagnetism and superconductivity fluctuation in pure highly oriented pyrolytic graphite [2,3], superconductivity in hole- or electron-doped C_{60} [4], ferromagnetism in rhombohedral C_{60} treated under high pressure and high temperature [5], complex magnetic behavior and high-pressure effects on structural and electronic properties in glassy carbon [6–8], etc. It is indicated that the ferromagnetic and superconducting properties could be ascribed to structural instability, supported by some theoretical studies [9,10]. Here it is noted that pressure plays a significant role in treating these carbon based materials or tuning their properties.

As one of non-crystalline carbon forms, activated carbon could be used as an absorption material and catalyst due to its porosity and surface chemistry activity. Activated carbon is composed of micrographites in the nanometer scale with short-range order [1]. The micrographite is formed with the stack of nano-sized graphitic sheets. So the study of activated carbon is helpful to understand the properties of nano-sized materials. There may be a magnetic ordering arrangement in the zigzag edge of graphitic sheets and micrographites that are made of several sheets [11,12]. The sheets and micrographites have other special properties in electronic transportation, optical spectra, field emission, etc [13–15]. So activated carbon should have novel properties due to its special structure.

Activated carbon could become graphite under high temperatures, like most amorphous carbon materials [16]. The graphitization temperature of activated carbon would reach above 2500 °C at ambient conditions [17]. High pressure can significantly reduce the graphitization temperature and substantially accelerate the kinetics of transformation of activated carbon and other non-crystalline carbon [18]. Inagaki et al. have reported that non-graphitized carbons can become graphite at ∼1500–1700 °C and 0.5 GPa [19–21]. High pressure could confine the micrographites of activated carbon in a fixed small space while high temperature diffusion could have them connect to each other, which accelerates the transition from activated carbon to graphite. The connections include the joint of graphitic sheets in the direction parallel with *c*-axis with Van der Waals force between graphitic sheets and the joint of sheets in the *ab*-plane with covalence bond between carbon atoms. Some oxide catalysts could also reduce the graphitization temperature of activated carbon but bring some impurities to the sample [22]. Activated carbon treated under high pressure and high temperature would be pure and useful for further research and application.

* Corresponding author. Tel.: +86 10 82648041; fax: +86 10 82640223.
E-mail address: zhaojg@aphy.iphy.ac.cn (J.G. Zhao).

0038-1098/$ – see front matter © 2009 Published by Elsevier Ltd
doi:10.1016/j.ssc.2008.12.027

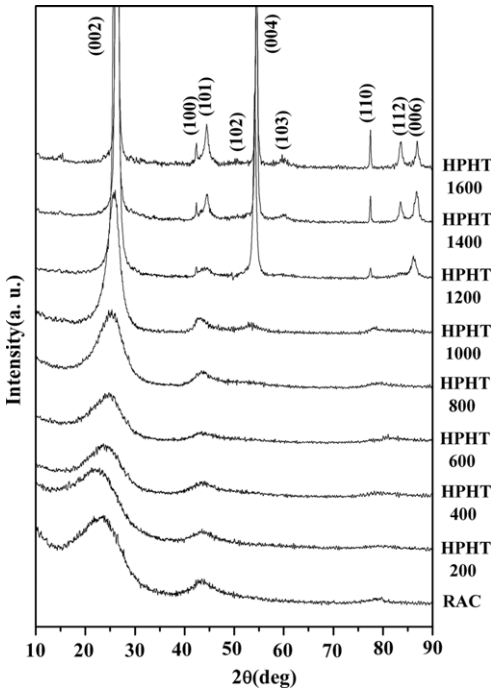

Fig. 1. The XRD patterns for activated carbon prepared at 5.0 GPa and different temperatures. The RAC represents the raw activated carbon.

In this communication, we have treated activated carbon powder by using high-pressure sintering, and examined the structural properties of these samples with x-ray diffraction (XRD) patterns, scanning electron microscope (SEM) photographs, and Raman spectra.

2. Experimental

A conventional cubic-anvil type high-pressure facility was used to perform the high-pressure and high-temperature treatments on activated carbon. The raw material, wrapped with a column of platinum foil of 5.0 mm in diameter to avoid contamination, was put into an h-BN sleeve which was in turn inserted into a graphite tube heater. Pyrophyllite was used as the pressure-transmitting medium, which can provide a good quasi-hydrostatic environment. The treating process was carried out at 5.0 GPa and 100–1600 °C for 5–10 min, where the rate of loading pressure is about 0.3 GPa/min below 1 GPa and is about 0.8 GPa/min above 1 GPa, and the rate of raising the temperature is about 100 °C/min. This was followed by a quench from high temperature before releasing pressure with the rate about 0.6 GPa/min. A detailed experimental technique can be found in Ref. [18]. While the sintering temperature exceeded 400 °C, the products were black and hard bulk. Here the samples are represented to HPHT+number with the number being the high-pressure sintering temperature. For example, the HPHT1600 denotes activated carbon treated at 5.0 GPa and 1600 °C. The structures of these samples were checked by the powder x-ray diffraction (XRD) technology with Cu-K_α radiation at room temperature, using a Rigaku diffractometer (MXP-AHP18) for $2\theta = 10°$–$90°$. The morphologies were observed through SEM photographs on a Hitachi S-4200. Raman spectra were collected through a micro-Raman spectrometer (Jobin Yvon T64000), by using a Verdi-2 solid-state laser (5320 Å) as the source for excitation, with the instrument resolution being 1 cm^{-1}.

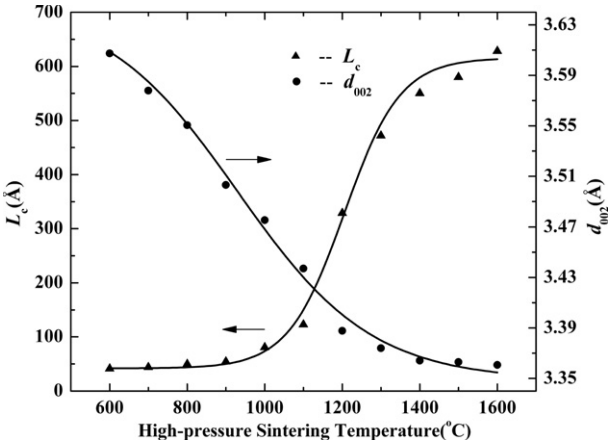

Fig. 2. The high-pressure sintering temperature dependencies of c-axis correlation length L_c and d spacing of peak (002) for activated carbon. The black bold lines are the Boltzmann fits to these data.

3. Results and discusion

The graphitization process of activated carbon under high pressure and high temperature can be reflected by x-ray diffraction patterns, as shown in Fig. 1. According to the peak intensity evolution, the graphitization process can be distinctly viewed in three regions. The non-graphitization region, near-graphitization region, and graphitization region correspond to activated carbon treated below 900 °C, at 1000–1100 °C, and above 1200 °C, respectively. There are only the peak (hk) and (002) in the XRD pattern of the raw activated carbon, which lacks other (hkl) peaks of graphite. While the high-pressure sintering temperature is below 1000 °C, activated carbon remains the non-crystalline form. With increasing high-pressure sintering temperature, the (hkl)-type peaks come forth gradually. To the samples in the near-graphitization region, the appearance of peak (004) indicates that the graphite phase begins to come into being, but the other peaks of graphite are still not found. Activated carbon becomes graphite at 1200 °C, while the peaks (101) and (006) begin to appear and the peaks (002) and (004) become very sharp. In this experiment, the graphitization temperature of activated carbon is lower than the previous results [17,19–21]. After graphitization, the (hkl)-type peaks (102), (103) and (112) appear. The c-axis correlation length L_c and d_{002} of HPHT600-1600 are calculated from the peak (002) by using the formula

$$L_c = 0.45\lambda/(\Delta \sin\theta) \quad (1)$$

and

$$d_{002} = \lambda/(2\sin\theta), \quad (2)$$

where λ is the wave length of incident x-rays, Δ is the half width, and θ is the diffraction angle [23]. The relationships of L_c and d_{002} versus high-pressure sintering temperature are shown in Fig. 2, and the data are fitted using the Boltzmann function. With increasing high-pressure sintering temperature, L_c increases and d_{002} decreases. There is a drastic increase of L_c in the range 1100–1300 °C, corresponding to the transition from the near-graphitization region to the graphitization region. The decrease of the d value at higher high-pressure sintering temperatures indicates that graphitic layers connect to each other more closely.

In the graphitization process of activated carbon, the morphology evolution with increasing high-pressure sintering temperature is observed using the SEM photographs. The raw activated carbon is made of anomalistic carbon grains with size about several microns, as shown in Fig. 3(a). While the high-pressure sintering temperature is below 600 °C, activated carbon is still made

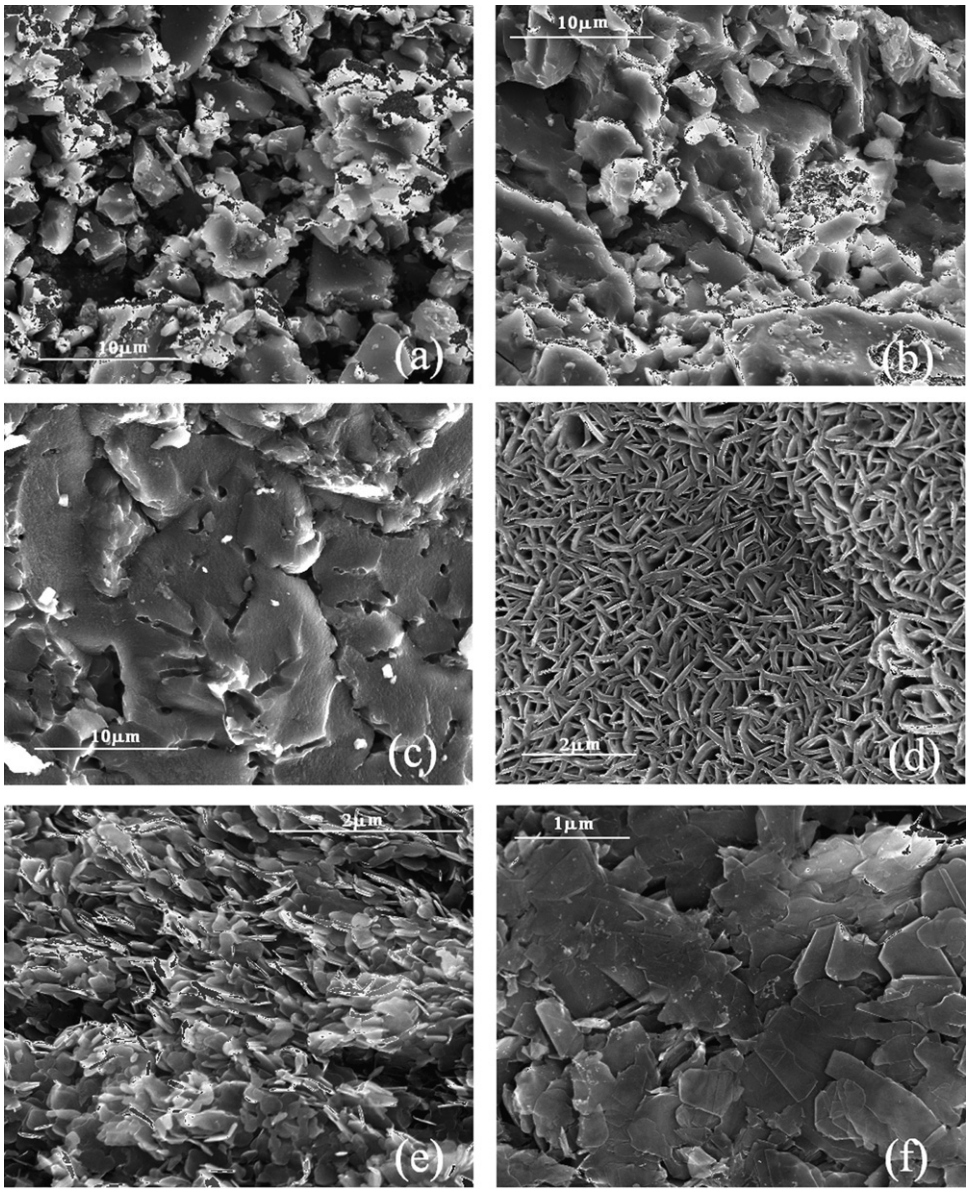

Fig. 3. SEM photographs of (a) the raw material and activated carbon treated at (b) 700 °C, (c) 900 °C, (d) 1100 °C, (e) 1200°C, (f) 1600 °C.

of small grains. The carbon grains become larger with increasing high-pressure sintering temperature and begin to merge together at 700 °C, as shown in Fig. 3(b). The SEM photograph of HPHT900 in Fig. 3(c) exhibits a high-extent of merged grains. The merged grains could be reflected by the acuity of the peak (002) in XRD patterns. To HPHT1000 and HPHT1100, the appearance of a honeycomb-like structure shows the drastic change in the texture, with the result of HPHT1100 being shown in Fig. 3(d). These results could correspond to the appearance of peak (004) in XRD patterns. The micrograph indicates that the higher sintering temperature strengthens the combination among carbon grains. The interior micrographites connect each other more closely at higher high-pressure sintering temperatures. However, the change of density is not obvious, as calculated from d_{002} through the formula [24]

$$\delta_{\text{x-ray}} = \frac{ZAm_{\text{H}}}{a_c^2 c\sqrt{3/2}} = \frac{7.627}{d_{002}}, \tag{3}$$

where $Z = 4$ is the number of carbon atoms in a unit cell, $A = 12$ is the atomic weight of carbon, $m_H = 1.66 \times 10^{-24}$ g is the mass of a hydrogen atom, and $a_c = 2.456$ Å is the lattice constant of graphite. In other words, there is only a little volume change for activated carbon from the non-graphitization region to the near-graphitization region. The micron-scale graphite-like ribbons and holes constitute the near-graphitization activated carbon. The combination among carbon grains enlarges the holes, which results in that the sample is asymmetric on the micron scale. Compared with graphite, it is more difficult to compress the material made of graphite-like ribbons due to its larger bulk modulus [7], and the holes remain in the sample under high pressure and high temperature. So there is a perforated structure in HPHT1000 and HPHT1100. When the high-pressure sintering temperature exceeds 1200 °C, slice-like structures begin to form, with the micrographs of HPHT1200 and HPHT1600 being shown in Fig. 3(e) and (f), respectively. The average size of these slices is tens of nanometers in thickness, which is approximately equal to the c-axis correlation length L_c. With increasing high-pressure sintering temperature, the area and thickness of the slices both increase after graphitization, which indicates that these graphitic slices become larger.

Fig. 4 gives the Raman spectra of activated carbon treated under different high-pressure sintering temperatures. The solid and

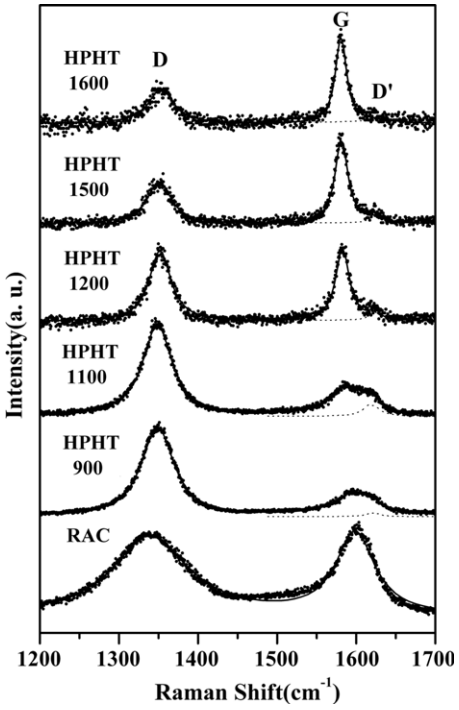

Fig. 4. First-order Raman spectra for the raw material and activated carbon treated at 5.0 GPa and various temperature. The solid line is the Lorentzian fit to these data and the dashed line is the fit to the ∼1620 cm^{-1} lines.

dashed lines represent the Lorentzian fit to the whole experimental data and the results near 1620 cm^{-1}, respectively. We could observe that there are two main first-order Raman modes at ∼1580 cm^{-1} and ∼1350 cm^{-1}. The 1580 cm^{-1} mode (G line) corresponds to the Raman-allowed E_{2g} mode in the ideal graphite, and the 1350 cm^{-1} mode (D line) corresponds with the disorder-induced line, which associates with the large density of phonon states. The weak 1620 cm^{-1} mode (D′ line) is also induced by disorder but associates with the density of mid zone phonon states [25]. Before graphitization, the intensity of G line in Raman spectra is weak and that of D line is strong, so there are a few crystals in these samples, which could be checked by XRD patterns and SEM photographs. After graphitization, the intensity of the G line begins to strengthen, but that of the D line is still strong, which indicates there are also disordered structures, being similar to the result in Ref. [26]. It should be emphasized that the spot diameter of the focused laser beam is about 1 μm, so the sample in this range contains many graphitic slices, even in the graphitized activated carbon, indicated by the SEM photographs. The edges of graphitic slices, including both armchair and zigzag edges, result in the formation of D and D′ modes [27,26]. In our samples, the arrangement of edges in the range of laser beam is disordered, which leads to D and D′ lines in Raman spectra. With increasing high-pressure sintering temperatures, the G line moves to the low-frequency direction.

4. Conclusions

High pressure can accelerate the graphitization process of activated carbon, with the graphitization temperature as low as 1200 °C at 5.0 GPa, indicated by XRD patterns. With increasing high-pressure sintering temperature, the texture of activated carbon changes from dispersive or merged carbon grains across honeycomb-like structures in the near-graphitization region to slice-like structures after graphitization. Raman spectra reflect that there are still some disorder structures in the graphitizated activated carbon.

Acknowledgements

We thank Prof. C. Dong and H. Chen for their help in XRD analysis.

References

[1] J. Robertson, Adv. Phys. 35 (1986) 317.
[2] Y. Kopelevich, P. Esquinazi, J.H.S. Torres, S. Moehlecke, J. Low. Temp. Phys. 119 (2000) 691.
[3] H. Kempa, Y. Kopelevich, F. Mrowka, A. Setzer, J.H.S. Torres, R. Höhne, P. Esquinazi, Solid State Commun. 115 (2000) 539.
[4] A.F. Hebard, M.J. Rosseinsky, R.C. Haddon, D.W. Murphy, S.J. Glarum, T.T.M. Palstra, A.P. Ramirez, A.R. Kortan, Nature 350 (1991) 600.
[5] T.L. Makarova, B. Sundquist, R. Höhne, P. Esquinazi, Y. Kopelevich, P. Scharff, V.A. Davydov, L.S. Kashevarova, A.V. Rakhmanina, Nature 413 (2001) 716.
[6] X. Wang, Z.X. Liu, Y.L. Zhang, F.Y. Li, R.C. Yu, C.Q. Jin, J. Phys.: Condens. Matter 14 (2002) 10265.
[7] X. Wang, Z.X. Bao, Y.L. Zhang, F.Y. Li, R.C. Yu, C.Q. Jin, J. Appl. Phys. 93 (2003) 1991.
[8] C.Q. Jin, X. Wang, Z.X. Liu, Y.L. Zhang, F.Y. Li, R.C. Yu, Braz. J. Phys. 33 (2003) 723.
[9] J. González, F. Guinea, M.A.H. Vozmediano, Phys. Rev. B 63 (2000) 134421.
[10] K. Harigaya, J. Phys.: Condens. Matter 13 (2001) 1295.
[11] M. Fujita, K. Wakabayashi, K. Nakada, J. Phys. Soc. Japan. 65 (1996) 1920.
[12] K. Nakada, M. Fujita, Phys. Rev. B 54 (1996) 17954.
[13] K. Nakada, M. Igami, M. Fujita, J. Phys. Soc. Japan. 67 (1998) 2388.
[14] K. Wakabayashi, M. Fujita, H. Ajiki, M. Sigrist, Phys. Rev. B 59 (1999) 8271.
[15] C.W. Chiu, F.L. Shyu, C.P. Chang, R.B. Chen, M.F. Lin, J. Phys. Soc. Japan. 7 (2) (2003) 170.
[16] R.E. Franklin, Proc. Roy. Soc. A 209 (1951) 196.
[17] Y. Hishiyama, M. Inagaki, S. Kimura, S. Yamada, Carbon 12 (1974) 249.
[18] X. Wang, G.M. Zhang, Y.L. Zhang, F.Y. Li, R.C. Yu, C.Q. Jin, G.T. Zou, Carbon 41 (2003) 188.
[19] M. Inagaki, A. Oberlin, S. de Fonton, High Temp.-High Press. 9 (1977) 453.
[20] M. Inagaki, S. Naka, J. Mater. Sci. 10 (1975) 814.
[21] T. Noda, K. Kamika, M. Inagaki, J. Chem. Soc. Japan. 41 (1968) 485.
[22] I. Mochida, R. Ohtsubo, K. Takeshita, Carbon 18 (1980) 117.
[23] M.A. Short, P.L. Warlker, Carbon 1 (1963) 3.
[24] M.M. Dubinin, G.M. Plavnik, E.D. Zaverina, Carbon 2 (1964) 261.
[25] R.J. Nemanich, S.A. Solin, Phys. Rev. B 20 (1979) 392.
[26] K. Kuriyama, M.S. Dresselhaus, J. Mater. Res. 4 (1992) 940.
[27] L.G. Cancado, M.A. Pimenta, B.R.A. Neves, M.S.S. Dantas, A. Jorio, Phys. Rev. Lett. 93 (2004) 247401.